The origin of the occurrence rate profile of gas giants inside 100 d

Mohamad Ali-Dib,[1,2]★ Anders Johansen[3] and Chelsea X. Huang[1,4,5]

[1]*Centre for Planetary Sciences, Department of Physical and Environmental Sciences, University of Toronto at Scarborough, Toronto, ON M1C 1A4, Canada*
[2]*Canadian Institute for Theoretical Astrophysics, 60 St. George St, University of Toronto, Toronto, ON M5S 3H8, Canada*
[3]*Lund Observatory, Department of Astronomy and Theoretical Physics, Lund University, Box 43, SE-22100 Lund, Sweden*
[4]*Dunlap Institute, University of Toronto, Toronto, ON, M5S3H4, Canada*
[5]*Juan Carlos Torres Fellow, MIT Kavli Institution, Cambridge, MA, 02139, USA*

ABSTRACT

We investigate the origin of the period distribution of giant planets. We fit the bias-corrected distribution of gas-giant planets inside 300 d found by Santerne et al. using a planet formation model based on pebble accretion. We investigate two possible initial conditions: a linear distribution of planetary seeds, and seeds injected exclusively on the water and CO icelines. Our simulations exclude the linear initial distribution of seeds with a high degree of confidence. Our bimodal model based on snowlines gives a more reasonable fit to the data, with the discrepancies reducing significantly if we assume the water snowline to be a factor of 3–10 less efficient at producing planets. This model moreover performs better on both the warm/hot Jupiters ratio and a Gaussian mixture model as comparison criteria. Our results hint that the gas-giant exoplanets population inside 300 d is more compatible with planets forming preferentially at special locations.

Key words: planets and satellites: formation.

1 INTRODUCTION

Variations in the period distribution of giant planets can provide a wealth of information on planet formation scenario. Classical planet formation models predict that giant planets should be more abundant outside of the snowline due to higher isolation masses caused by higher solids density (Pollack et al. 1996). Planets, however, can interact with the disc via torques exerted by the spiral arms induced by the planet, and these can push the planet significantly in either radial direction (Kley & Nelson 2012). Moreover, a giant planet can interact with other giant planets or stellar companions, possibly scattering the planet off. These processes are sensitive to the disc's thermal and density structure, and the presence and properties of these other massive companions. Constraining formation models with period distribution observations is hence crucial, but becoming increasingly possible now with new data influx.

The variation in the period distribution of giant planets is first noticed in radial velocity surveys. Udry, Mayor & Santos (2003) first mentioned a period valley between 10 and 100 d. This period valley sits between the hot Jupiters (HJs)[1] pile-up at short periods (3–4 d) and warm Jupiters (WJs) beyond 100 d. We note that WJs are defined here as giant planets orbiting on periods between 10 and 300 d, slightly beyond the common definition ending at 100 d. A similar period distribution is seen in transiting giant planets observed by the

Kepler mission, although the strength of the HJ pile-up may differ slightly from those from the radial velocity surveys (Howard et al. 2012; Dawson & Murray-Clay 2013). One difficulty of estimating the occurrence rate of giant planets from *Kepler* is the relatively large false positive rate. Santerne et al. (2016) combined ground-based radial velocity follow up results with a magnitude-limited sample of giant planets discovered by *Kepler* and reported the occurrence distribution of giant planets with orbital period smaller than 300 d around FGK stars. They found a HJ occurrence rate about half of what is found by the radial velocity surveys (Marcy et al. 2005; Wright et al. 2012), and confirmed a similar deficit of planets outside the period valley starting at 10 d orbits.

A summary of Santerne et al. (2016) results is plotted in Fig. 1, showing the occurrence rate of the different giant planets classes as a function of the orbital period. We notice mainly the HJs pile-up at 3 d and the dip in the occurrence rate around 10 d, where HJs end and WJs start. In total, WJs outnumber the HJs population significantly.

Classical population synthesis models (Ida & Lin 2004; Mordasini, Alibert & Benz 2009) were successful in reproducing multiple aspects of exoplanets statistics, for example the high occurrence rate of small planets, the planet–star metallicity correlation and the low occurrence rate of intermediate mass planets. These models were however unable to reproduce the HJs pile-up at 3 d, and attributed this to the migration scheme used (Benz et al. 2014; Mordasini et al. 2015). This pile-up however was reproduced by Beaugé & Nesvorný (2012) through high eccentricity migration of planets placed in systems with three or four planets starting at mean motion

★ E-mail: m.alidib@utoronto.ca
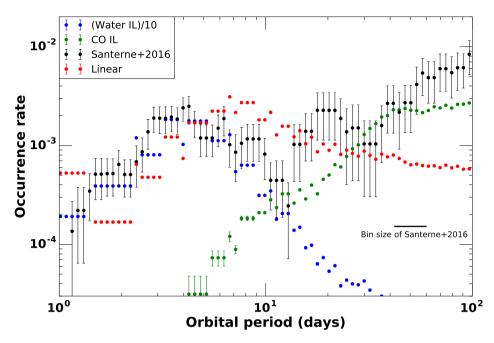[1] Planets on orbits shorter than 10 d.

Figure 1. The occurrence rate (per star) of giant (Jovian) planets as a function of their semi-major axis from Santerne et al. (2016). Note that to resolve the dip around 10 d period better, we plot the occurrence rate in a sliding bin, in which each data point and its error bars represent the occurrence rate and uncertainties in a bin centred at this data point in logarithmic space, and with bin width of 0.2333. We fit this distribution with two planet formation models. In the linear model, planetary seeds are injected randomly throughout the disc. In the bimodal model, seeds are injected solely at the water and CO icelines positions. The linear case leads to a near-constant occurrence rate of gas giants, while the bimodal case is more compatible with observation. The bimodal case moreover predict a WJ/HJ ratio significantly closer to observations.

resonances. Wu & Lithwick (2011) on the other hand proposed that this pile-up can be explained by secular chaos in systems with three giant planets. All of these models, however, do not try to reproduce the dip in the occurrence rate of gas giants at 10 d.

In this work, we offer an alternative explanation to the gas-giants occurrence rate profile by fitting it to a populations synthesis model based on pebble accretion. The goal is to check multiple families of initial conditions and compare them to the observations. Specifically, we want to understand whether this population is recovered better from a stochastic linear distribution of planetary seeds, or if formation only at special locations in the disc is needed to retrieve the bimodal distribution seen in Fig. 1. Our model has the advantage of recovering the occurrence rate details entirely through disc migration.

2 MODEL

The model we use in this work is based on Ali-Dib (2017a,b), following Lambrechts & Johansen (2014), Lambrechts, Johansen & Morbidelli (2014), Bitsch, Lambrechts & Johansen (2015a), Bitsch et al. (2015b) and Morbidelli et al. (2015). It includes the following:

(i) Fits to a radiative 2D disc model with accurate opacities transitions leading to structures in the disc. We note however that since these simulations were done for a constant 1 solar mass star and a constant turbulent $\alpha \sim 5 \times 10^{-3}$, we do not vary these parameters to be consistent with the simulations.

(ii) Parametric pebbles and gas accretion including pebble accretion in both the Bondi and Hill regimes, in addition to slow and fast phases gas accretion.

(iii) Type I and II migration through torque evaluation. Type I migration will affect low mass planets through the Lindblad and corotation torques, while type II migration will affect planets mas-

sive enough to open a gap in disc and follow its viscous evolution. We assume that the planets inward migration will stop at the inner cavity, and hence will not be lost to the star. It is however important to note that we find no inner grid boundary pile-up of HJs, and thus the inner boundary condition have no effect on our model. Moreover, our inner visualization bin starts at 0.7 d (beyond the inner edge of the grid) to be consistent with Santerne et al. (2016).

(iv) Photoevaporation (PE) can increase the metallicity of the disc and thus affect its opacity. We assume a simplistic PE model, where we modify the accretion rate controlling the disc structure by reducing the PE mass flux from it till eventually it reaches 0 where the disc is assumed to be completely dispersed. PE will remove the disc's gas while retaining the dust, leading to gradual increase in its metallicity, which we integrate into the model (Guillot & Hueso 2006). We however do not take into account the viscous spreading of the disc due to PE. We are hence replacing the disc global accretion rate $\dot{M}_{\mathrm{acc}}$ of Bitsch et al. (2015b) by

$$\dot{M}' = \dot{M}_{\mathrm{acc}} - \dot{M}_{\mathrm{PE}}, \qquad (1)$$

and then define the disc's gas metallicity enhancement as

$$\varepsilon_c = 1 + \frac{\dot{M}_{\mathrm{PE}}}{\dot{M}_{\mathrm{acc}}} \qquad (2)$$

(v) Simulations are stopped when either the disc fully dispersed, or when the planet reach the inner edge of our disc at 0.01 au.

Moreover, we modified the model above to take into account the growth of small planetary seeds. In the earlier models, we injected seeds with masses $\sim 10^{-4}$ M$_\oplus$, close to the pebble transition mass, and their growth was dominated by pebble accretion. In this work, however, we start with smaller seeds with masses $= 10^{-5}$ M$_\oplus$ (corresponding the a radius of 160 km, in the same order of the observed bump in the asteroids size distribution Bottke et al. 2005), and

Table 1. Initial conditions.

Linear parameters	Range	
T_{ini}	10^5 yr – disc dissipation	
R_0	0.5–30 au	
Gaussian distributions	μ	σ
metal (per cent)	0.47	0.7
$\dot{M}_{FUV}$ ($M_\odot$/yr)	2×10^{-9}	2×10^{-9}
M_0 ($M_\oplus$)	10^{-5}	–
Z_0 (per cent)	$2 \times$ metal	–
f	0.2	–
κ_{env} (cm^2 g^{-1})	0.02	–
ρ_c (g cm^{-3})	5.5	–
H_2O iceline	150 K	–
CO iceline	25 K	–

hence we self-consistently incorporated the relevant weak coupling branch into the model. We hence follow Johansen et al. (2015), and Johansen & Lambrechts (2017) by defining the effective accretion radius in the Bondi regime as

$$\hat{R}_{acc} = \left(\frac{4\tau_f}{t_B} \right)^{1/2} R_B. \tag{3}$$

For the weak coupling branch ($\tau_f > t_B$ and $R_B < R_H$), we follow Ormel & Klahr (2010) in modifying this accretion radius as

$$\hat{R}_{acc} = \hat{R}_{acc} \times \exp(-0.4 \times (\tau_f/t_p)^{0.65}) \tag{4}$$

with the characteristic passing time-scale

$$t_p = GM/(\Delta v + \Omega R_H)^3. \tag{5}$$

Moreover, we also take into account planetesimal accretion that is important for seeds in this mass range, specially in the inner disc. We hence follow Bitsch et al. (2015b) in defining the corresponding accretion rate as

$$\dot{M}_{c,plan} = 3 \times 10^{-4} \left(\frac{10\,au}{r_p} \right) R_H v_H \Sigma_{peb}, \tag{6}$$

where v_H is the Hill velocity and Σ_{peb} is the pebble surface density.

Such a global model includes a large number of free parameters. To keep the problem tractable, we only vary the parameters that are assumed to affect directly the planets occurrence rates, shown in Table 1. The free parameter space is explored through a population synthesis approach. The seed injection time (T_{ini}) is drawn linearly, while the seed injection location (R_0) is drawn either linearly or bimodally (snowlines). The dust metallicity (in small coupled dust grains) and Z_0 (the pebble metallicity) on the other hand are drawn from a Gaussian distribution with the mean and standard deviation of the stars sample used in Santerne et al. (2016). The disc's FUV photoevaporative flux ($\dot{M}_{FUV}$) is also drawn from a Gaussian distribution reflecting the disc age distribution of Hernández et al. (2007). The rest of the problem's free parameters are assumed to be constant, including M_0 (the seed's initial mass), f (a fudge factor that reconciles our simplified slow phase gas accretion rate parametric fit with more detailed hydrodynamic simulations), κ_{env} (the envelope opacity) and ρ_c (the core's density). These parameters are explained more in detail in Bitsch et al. (2015b) and Ali-Dib (2017a).

2.1 Dynamical properties

The main caveat in this model is not taking into account the dynamical evolution of planets, even though half of the WJs in the RV sample (Wright et al. (2011) have significant eccentricities ($e \gtrsim 0.2$, and cf. The exoplanets.org data base[2]). This is problematic because disc–planet interactions are not expected to excite large eccentricities (Bitsch et al. 2013). Moreover, it is not clear why these planets have parked on these orbits instead of migrating all the way to become HJs.

On the other hand, even though eccentricities can be excited by planet–planet scattering, at small enough semi-major axes ($a \lesssim 0.5$ AU for a Jupiter-like planet) this will lead to planet–planet collision with small eccentricity excitation ($e \lesssim 0.1$; Ford et al. 2001; Johansen et al. 2012; Petrovich et al. 2014). One possible solution is planet–planet scattering during early dynamical instabilities (Lega, Morbidelli & Nesvorný 2013; Sotiriadis et al. 2016). Another possibility is based on the intriguing trend that WJs with outer planetary companions have a significantly wider eccentricity distribution than the sample without companions (Dong, Katz & Socrates 2014; Petrovich & Tremaine 2016). This sample could have undergone high-eccentricity migration (through Kozai oscillations followed by tidal circularization; Dawson & Chiang 2014). However, tides are too weak at these relatively wide orbits to be effective.

Petrovich & Tremaine (2016) proposed that this population is transient, where the planets are undergoing continuous migration from secular planet–planet or star–planet interactions, and we only observe them at the low eccentricity phase of this migration, and showed that such mechanism can reproduce their eccentricity distribution. Therefore, a fraction of WJs with the largest eccentricities ($e \gtrsim 0.4$) migrate through this mechanism, while the fraction with lower eccentricities migrate through another channel.

Another dynamical property of gas giants is their spin–orbit alignment (the angle between their orbital axis and the spin axis of their parent stars). However, there is virtually no constraints on the WJ population from spin–orbit angles. Although many of them are in multiple transiting planet systems (Huang, Wu & Triaud 2016), which are expected to be aligned with their host star. A notable exception is HD80606b (Winn et al. 2009) with 45° angle. For HJs, statistics from the exoplanets.org data base show a median absolute angle of 13.8° for this population. Therefore roughly 50 per cent of HJs have spin–orbit misalignment. Crida & Batygin (2014) however concluded that the spin–orbit misalignment of HJs is compatible these having been transported via disc migration in a disc torqued by a companion. In this case, both aligned and misaligned HJs could have formed on the snowline and then disc-migrated inward as per our model, explaining the pile-up observed in both populations (Winn & Fabrycky 2015).

3 RESULTS AND DISCUSSIONS

3.1 Analytical considerations

The gas giants occurrence rate profile in Fig. 1 is spread out over two orders of magnitude, and appears to be bimodal with a bell-like distribution inside 10 d and a power law beyond it. It is hard to imagine how to get such structure using a classical protoplanetary disc model with stochastic initial distribution of planetary seeds.

Let us assume a basic protoplanetary disc where temperature and density follow simple power laws. The solid accretion rate on to a

---

[2] Consulted on 2017 February 1.

core and its disc type I migration speed both scale linearly to the disc's density. Therefore, a random initial distribution of planetary embryos will lead to a near-constant final distribution of gas giants. In other words, if we inject enough planetary seeds (while exploring the entire free-parameter space) in the disc, we expect the resulting population of gas giants to occupy every possible final location, since all of the processes in this toy model are linear.

A possible way to generate this bimodal distribution is if planets form preferentially at specific locations in the disc. The most interesting permanent disc structures to consider are the main volatiles condensation fronts (snowlines). This is motivated theoretically by multiple works arguing that snowlines can be preferred places for planets formation (Ros & Johansen 2013; Ali-Dib et al. 2014; Ida & Guillot 2016; Schoonenberg & Ormel 2017), and observationally by the radial gaps seen in TW Hya (Andrews et al. 2016; Nomura et al. 2016) and HL Tau (ALMA Partnership et al. 2015), and their correlation with the positions of icelines (Zhang, Blake & Bergin 2015).

Since these are fundamentally temperature-dependent, their location will vary within the same disc with time as it cools down. If planet seeds form preferentially at two snowlines (water and CO, for example), then even with a completely linear disc, we might end up with a bimodal distribution.

3.2 Simulations

We first run simulations with linear initial distribution of planetary seeds (as shown in Table 1). Resulting occurrence rates as a function of period are presented in Fig. 1. This result conforms to what we expected in the analytical discussions, which is a quasi-linear final distribution of gaseous giant. The small bump inside 10 d can be attributed to type I migration. It is analogues to the overabundance in HJs found in the classical population synthesis models. This was attributed to short type I migration time-scale leading to a big pile-up of planets at the inner edge of the disc. Since our model incorporates the corotation torque, slowing down type I migration, in addition to the fast pebbles accretion (decreasing the time a planet will take to open a gap), the huge edge of the grid pile-up of classical population synthesis models translates into the mild pile-up at 8 d.

We now run simulations assuming that small planetary seeds form preferentially on the water and CO icelines. We hence inject the seeds exclusively at the (evolving) snowline positions, calculated via the disc model. The younger a disc is, the hotter it is and thus the farther the snowlines are. This will lead naturally to a bell-like occurrence rate for each snowline, resembling that seen in Fig. 1. This however works only if we give the two icelines different weights by reducing the planets formation efficiency rate of the water iceline by a factor between 3 and 10. We are hence assuming that either the water iceline forms planetary embryos less efficiently than we assumed, or that a significant fraction of its planets are lost to the star (Trilling et al. 1998; Hasegawa & Ida 2013).

The main result from our simulations is that a linear distribution of planetary embryos will lead to a quasi-linear final distribution of gas giants, while a bimodal distribution of seeds (on snowlines) will lead to 2 clusters. To understand more the physical origin of this let us consider the following simple case.

Let us fix the seed injection location for a planet to a specific radius in the disc, for example 10 au. The growth/migration track of this planet will depend on the disc temperature/density structure around and inside of 10 au. This disc structure is time dependent, so planets forming at 10 au at different times will encounter different
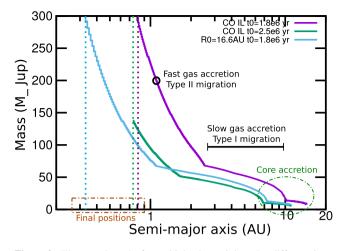

Figure 2. The growth tracks for multiple planets injected at different times and locations in the disc. The two tracks for the seeds injected at the CO iceline at different times converge to roughly the same location since they encountered similar disc density and temperature profiles due to starting at the same temperature. The seed injected at the same location where the iceline was but at a different time end up relatively far from the other two cases, since it encountered a different disc structure due to it starting at a different temperature.

disc structures and thus follow different growth tracks. Therefore, our 10 au seed, injected at different times in the disc, will end up at different locations. If we integrate this over all possible starting locations and disc free-parameters, the resulting gas giants will occupy every possible final location in the disc and thus lead to a quasi-linear occurrence rate profile.

On the other hand, let us imagine planetary seeds placed exclusively on a snowline. Since the snowline is a point in the temperature/density profile of the disc and not a fixed radius, planets forming at this point at different times will experience roughly similar density/temperature profiles inside their location and thus their formation tracks will converge around a specific location leading to clustering. This can be seen in Fig. 2.

We note that mixing the linear model with the CO iceline planets will lead to an occurrence rate profile that resemble somehow observations, but shifted to the right. This hence will fit neither the HJ pile-up or the dip at 10 d. It is however hard (if not impossible) to tweak the parameters in a way that makes this work. This is because the CO iceline planets will always have the same distribution controlled by the CO condensation temperature that is not a parameter. Thus, the only degree of freedom is the linear case planets. To push this distribution left, we need a cut-off in the possible initial location of planets at some orbital period. This seems unnatural within the physics included in the model. Moreover, it is not clear why there would be this cut-off, only to be followed further out by a very active CO iceline.

It is important to mention that all of our simulations are scalable vertically, meaning that, assuming statistical significance, we are allowed to multiply our occurrence rates by a constant value for the entire simulation. This is because we are trying to fit the relative occurrences rates of the different planetary populations, not the absolute abundance of gas giants.

3.3 The effects of the model's parameters

To better understand the effect of the different parameters explored in the population synthesis, we split the range used for each
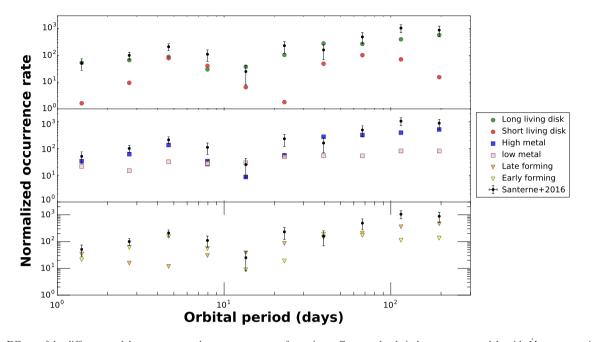
Figure 3. Effects of the different model parameters on the occurrence rate of gas giants. Green and red circles represent models with $\dot{M}_{FUV}$, respectively, less and more than 2×10^{-9} $M_{\odot}$ yr^{-1}. Blue and pink squares represent models with disc grain metallicity, respectively, higher or less than 0.47 per cent. Orange and yellow triangles correspond to models with planets seed injection times of, respectively, more and less than 2 Myr. We notice that the occurrence rate is higher for planets either forming early, or in long living discs, or in discs with high metallicity. This is expected since these conditions favour the formation of gas giants who need enough metals and a lot of time to form.

parameter into two halves at the median value, and visualize the occurrence rate for each of them. The photoevaporative mass flux will affect a disc's dispersal time and metallicity. Discs with lower PE mass fluxes will live longer, thus giving more time for giant planets to form. We hence expect this parameter to affect the giant planets distribution by increasing the occurrence rates for lower fluxes. The disc metallicity on the other hand controls the amount of solids available for planets formation. Moreover, it affects the disc structure through opacity. To first order, due the planet–star metallicity correlation (Fischer & Valenti [2005](); Guillot et al. [2006]()), we expect discs with higher metallicities to be more efficient at forming planets. Results of parameters exploration are shown in Fig. [3](). We notice that the occurrence rate of gas giants is dominated by high metallicity and long living discs. This is not surprising since these parameters give a gas giant enough solid materials and time to form. The effect of when did a planet start forming in the disc (early versus late) is less trivial, since forming early will give a planet more time to evolve into a gas giant, but also will affect where it is going to end up in the disc. This non-linear effect is the reason why CO iceline planets are dominated by planets forming late in the disc. Interestingly, we notice that the overall occurrence rate shape (width and depth) is robust to the explored parameters ranges. This indicate that this shape is controlled by the underlying physical model and its implicit assumptions (accretion and migration speeds, disc model), rather than by our choice of parameters. Other -fixed- parameters (icelines temperatures and core density) are invariable physical quantities that will not differ between systems. The effect of the only remaining parameter, envelope opacity, is shown in Fig. [4](). This plot compares the occurrence rates for identical models with two different envelope opacity parameter: 0.02 and 0.05 cm^2 g^{-1}. The effect of this change is minimal, with the depth and width of the profile unchanged for both water and CO iceline planets.

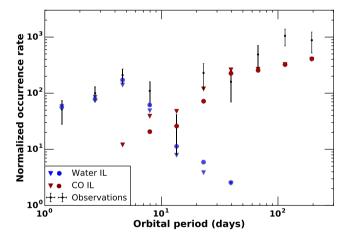**Figure 4.** The effect of the envelope opacity on the occurrence rate of gas giants. Circles represent our nominal opacity case (0.02 cm^2 g^{-1}) and triangles represent higher opacity (0.05 cm^2 g^{-1}). The differences between the two cases are minimal.

3.4 WJ/HJ ratio

A more general and bin-size independent method of comparing the models to data is through the WJs to HJs occurrence rates ratio (W/H). This should give basic but solid information on the accuracy of the models in reproducing the relative abundances of the two giant planets population. We hence calculate this ratio (where HJs are inside 10 d and WJs are beyond this) for the observational data and the two models. From Santerne et al. ([2016]()), the data W/H is ~ 8.3. The linear model on the other hand gives a W/H of ~ 1. This near-unity value implies that the linear model predicts

as many HJs as WJs, which is expected from the analytic considerations, and from the fact that even though the WJs space is larger, the inner disc (translating into HJs) is more efficient at forming planets.

The icelines model gives a W/H ∼ 8 only after decreasing the efficiency of the water iceline by a factor of 10. The icelines case provides fit better than linear case for water iceline efficiency ranging from 1.25 (where it leads to W/H=1) to 10, where it matches observations.

This moreover can be improved if we assume that the 50 per cent of WJs with high eccentricities all formed via dynamical instead of disc migration. This therefore can allow us to decrease the data W/H to ∼ 4, and thus fit the data perfectly by reducing the water iceline efficiency by a factor of 5. This however does not take into effect HJ who might have reached their current orbits via high eccentricity migration followed by tidal circularisation. If this population is significant, then this will increase the measured W/H ratio back to near 8.

This implies that our model either overestimates the abundances of HJs, or underestimate the abundance of WJs. In the first case scenario, our model would be similar to the earlier population synthesis models that predicted a pile-up of HJs due to type I migration. In the second case scenario, an additional source of WJs might be needed. Other structures in the disc can possibly play this role. For example, the N_2 iceline should be close to the CO iceline since the two elements condense at comparable temperatures (Fray & Schmitt 2009). A significant fraction of planets forming at this location should therefore end up as WJs, in parallel with the CO iceline planets. Another possible location is the outer edge of the deadzone, where the viscosity transition can trigger a Rossby wave instability (Lyra et al. 2009), leading to an accumulation of solids that might trigger planets formation.

3.5 Statistical analysis

To test the statistical significance of our findings, we conduct a Gaussian Mixture Model (GMM) analysis that predicts the optimal number of Gaussian components that fit the data and the simulations. Models with low Bayesian information criteria (BIC) value are preferred to those with higher values (Hastie, Tibshirani & Friedman 2013).

Our results in Fig. 5 show that the observational data significantly favour two Gaussian components over one, and so does both the Icelines and linear cases. However, the icelines case have a steeper slope between 1 and 2 components than the linear case, implying that it prefers two components more strongly than the linear case, thus favouring it as a fit to the data.

The ratio between the BIC score for a two component/multicomponent GMM model and a one component GMM model tells us about the significance of how bimodal/multimodal the data is. In our particular case, the iceline model and observational data are both more strongly bimodal when compared to the linear model, because the slope of their BIC is steeper between 1 and 2 components. This is different from the standard KS tests because these are most sensitive when the underline distributions differ in a global fashion near the centre of the distribution. However, it is possible to make centres of distribution similar between a single mode and a bimodal distribution. Since, we are more interested in if the giant population is bimodal, a BIC test with GMM model is more appropriate compared to a KS test.
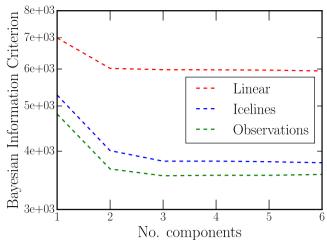

Figure 5. GMM analysis for the observational data and two models. We notice that the information gain (BIC decrease) from 1 to 2 components model is greater for the observations and icelines model than for the linear model. This implies that the observations and icelines model are both more strongly bimodal than the linear case.
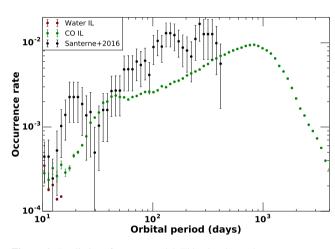

Figure 6. Predictions from our model. This plot shows the occurrence rate of gas giants beyond 100 d as predicted by our icelines model. These planets all started forming at the CO iceline. We predict that, similar to the water iceline planets, the CO iceline planets will follow a bell-like occurrence rate profile, with a central pile-up and smooth decrease on both sides.

3.6 Predictions

Our predictions from this model are show is Fig. 6. Since in our model planets form exclusively on the water and CO icelines, and since both follow the same physics, we expect the occurrence rates of gas giants generated by the two icelines to follow similar profiles. This is validated by the simulations, where CO iceline gas giants follow a bell-like distribution with a central pile-up. We predict this pile-up to be no further than 1000 d orbits, followed by a steady decline.

4 SUMMARY AND CONCLUSIONS

In this work, we investigated the origin of the occurrence rate radial profile of gas-giants inside 300 d found by Santerne et al. (2016). We used a population synthesis model based on pebble accretion including solids and gas accretion, disc migration and simplified PE to fit the observational data. Starting from a linear distribution of

planetary seeds uniform throughout the disc, our simulations produce a quasi-linear final distribution of planets with a near unity WJ/HJ ratio, and thus fail to properly fit the data. If we inject planetary seeds solely on the water and CO icelines however, we get a much better statistical fit, assuming a factor of 3–10 lower efficiency for the water IL. Moreover, we conducted a GMM analysis showing that the icelines model is more strongly bimodal than the linear model, indicating that it is a better fit to the firmly bimodal data. Our results exclude simple models with linear initial distribution of planetary seeds, and hint towards snowlines being preferred places for planets formation. Our model can be improved on multiple fronts. The most significant missing element is planetary dynamics. In this model, we use disc migration to move planets forming on icelines inward to where they are observed. We however do not see any fundamental reason why these planets cannot form at the icelines and then migrate dynamically inwards via Kozai/scattering/secular migration, thus explaining the eccentricities of WJs. These are highly non-linear effect that needs detailed modelling. Another possible relevant effect is snowline fossilization (Morbidelli et al. 2016) that becomes important when forming multiple gas giants in a single disc.

ACKNOWLEDGEMENTS

REFERENCES

Ali-Dib M., 2017a, MNRAS, 467, 2845
Ali-Dib M., 2017b, MNRAS, 464, 4282
Ali-Dib M., Mousis O., Petit J.-M., Lunine J. I., 2014, ApJ, 793, 9
ALMA Partnership et al., 2015, ApJ, 808, L3
Andrews S. M. et al., 2016, ApJ, 820, L40
Beaugé C., Nesvorný D., 2012, ApJ, 751, 119
Benz W., Ida S., Alibert Y., Lin D., Mordasini C., 2014, in Beuther H., Klessen R. S., Dullemond C. P., Henning T., eds, Protostars and Planets VI, Univ. Arizona Press, Tucson, AZ, p. 691
Bitsch B., Crida A., Libert A.-S., Lega E., 2013, A&A, 555, A124
Bitsch B., Lambrechts M., Johansen A., 2015a, A&A, 582, A112
Bitsch B., Johansen A., Lambrechts M., Morbidelli A., 2015b, A&A, 575, A28
Bottke W. F., Durda D. D., Nesvorný D., Jedicke R., Morbidelli A., Vokrouhlický D., Levison H., 2005, Icarus, 175, 111
Crida A., Batygin K., 2014, A&A, 567, A42
Dawson R. I., Chiang E., 2014, Science, 346, 212
Dawson R. I., Murray-Clay R. A., 2013, ApJ, 767, L24
Dong S., Katz B., Socrates A., 2014, ApJ, 781, L5
Fischer D. A., Valenti J., 2005, ApJ, 622, 1102
Ford E. B., Havlickova M., Rasio F. A., 2001, Icarus, 150, 303
Fray N., Schmitt B., 2009, Planet. Space Sci., 57, 2053
Guillot T., Hueso R., 2006, MNRAS, 367, L47
Guillot T., Santos N. C., Pont F., Iro N., Melo C., Ribas I., 2006, A&A, 453, L21
Hasegawa Y., Ida S., 2013, ApJ, 774, 146
Hastie T., Tibshirani R., Friedman J., 2013 The elements of Statistical Learning, 2nd edn
Hernández J. et al., 2007, ApJ, 662, 1067
Howard A. W. et al., 2012, ApJS, 201, 15
Huang C., Wu Y., Triaud A. H. M. J., 2016, ApJ, 825, 98
Ida S., Guillot T., 2016, A&A, 596, L3
Ida S., Lin D. N. C., 2004, ApJ, 604, 388
Johansen A., Lambrechts M., 2017, AREPS, in press
Johansen A., Davies M. B., Church R. P., Holmelin V., 2012, ApJ, 758, 39
Johansen A., Mac Low M.-M., Lacerda P., Bizzarro M., 2015, Sci. Adv., 1, 1500109
Kley W., Nelson R. P., 2012, ARA&A, 50, 211
Lambrechts M., Johansen A., 2014, A&A, 572, A107
Lambrechts M., Johansen A., Morbidelli A., 2014, A&A, 572, A35
Lega E., Morbidelli A., Nesvorný D., 2013, MNRAS, 431, 3494
Lyra W., Johansen A., Zsom A., Klahr H., Piskunov N., 2009, A&A, 497, 869
Marcy G. W., Butler R. P., Vogt S. S., Fischer D. A., Henry G. W., Laughlin G., Wright J. T., Johnson J. A., 2005, ApJ, 619, 570
Morbidelli A., Lambrechts M., Jacobson S., Bitsch B., 2015, Icarus, 258, 418
Morbidelli A. et al., 2016, Icarus, 267, 368
Mordasini C., Alibert Y., Benz W., 2009, A&A, 501, 1139
Mordasini C., Mollière P., Dittkrist K.-M., Jin S., Alibert Y., 2015, Int. J. Astrobiology, 14, 201
Nomura H. et al., 2016, ApJ, 819, L7
Ormel C. W., Klahr H. H., 2010, A&A, 520, A43
Petrovich C., Tremaine S., 2016, ApJ, 829, 132
Petrovich C., Tremaine S., Rafikov R., 2014, ApJ, 786, 101
Pollack J. B., Hubickyj O., Bodenheimer P., Lissauer J. J., Podolak M., Greenzweig Y., 1996, Icarus, 124, 62
Ros K., Johansen A., 2013, A&A, 552, A137
Santerne A. et al., 2016, A&A, 587, A64
Schoonenberg D., Ormel C. W., 2017, A&A, 602, A21
Sotiriadis S., Libert A.-S., Bitsch B., Crida A., 2016, A&A, 598, a70
Trilling D. E., Benz W., Guillot T., Lunine J. I., Hubbard W. B., Burrows A., 1998, ApJ, 500, 428
Udry S., Mayor M., Santos N. C., 2003, A&A, 407, 369
Winn J. N., Fabrycky D. C., 2015, ARA&A, 53, 409
Winn J. N. et al., 2009, ApJ, 703, 2091
Wright J. T. et al., 2011, PASP, 123, 412
Wright J. T., Marcy G. W., Howard A. W., Johnson J. A., Morton T. D., Fischer D. A., 2012, ApJ, 753, 160
Wu Y., Lithwick Y., 2011, ApJ, 735, 109
Zhang K., Blake G. A., Bergin E. A., 2015, ApJ, 806, L7

This paper has been typeset from a TEX/LATEX file prepared by the author.